DEPOSITION AND CHARACTERIZATION OF DOPAMINE AND POLYDOPAMINE THIN FILMS: MODIFIERS FOR ELECTRICAL CONTACTS IN PEROVSKITE SOLAR CELLS

By

LEO MARC HAMERLYNCK

_____

A Thesis Submitted to The Honors College

In Partial Fulfillment of the Bachelors degree
With Honors in

Chemistry

THE UNIVERSITY OF ARIZONA

M A Y 2 0 1 8

Approved by:

_____

Dr. Neal Armstrong

Department of Chemistry & Biochemistry

Table of Contents

Abstract

This work details the preparation and characterization of dopamine (Dop) and BOC-protected polydopamine (pDop) modification of TiO_2 prepared by CVD as an interlayer for interfacial control of crystalline order and stability in mixed-halide formamidinium lead halide perovskites, an exciting light-harvesting material for thin-film photovoltaics. Dop and pDop modification is achieved by spin-coating from pH-adjusted aqueous solutions and rinsing with DMSO/DMF. Morphology of the films is studied by atomic force microscopy (AFM), showing conformal coating by pDop and preferential binding to chemically active TiO_2 sites by Dop. The films are characterized by infrared reflection-absorption spectroscopy (IRRAS) and photoelectron spectroscopy (PES), and the surface energetics show a positive surface dipole and increased hole blocking capacity in pDop, both promising for a device interlayer. The effect of these modifications on perovskite growth, morphology, and crystallinity, is determined by X-ray diffraction (XRD) and AFM, showing an increase in perovskite crystallinity (due to surface passivation) on both Dop- and pDop-modified TiO_2, and an unusual crystal orientation induced by pDop modification. A novel IR spectroscopic characterization of formamidinium in perovskite, probing disordered formamidinium at grain boundaries and crystalline domain interfaces is presented, improving on the current state of the literature.

I. Introduction

Hybrid organic-inorganic lead halide perovskite (PVSK) materials are an exciting and relatively new material for use in sunlight harvesting in thin-film photovoltaic (PV) devices (or solar cells). This excitement is due in large part to the rapidly growing power conversion efficiencies of PV devices incorporating these materials, from just above 3% in 2009 (the first reported use of PVSK in a PV device)[1] to above 22% as certified by the National Renewable Energy Laboratory (NREL) in 2018, putting these devices on the same order of efficiency as conventional silicon solar cells.[2] Unlike silicon solar cells, thin-film PV devices can be solution- or vapor-processed at low temperature and pressure, potentially allowing for a much lower manufacturing cost. The excellent performance of PVSK materials in these devices owes itself to their many desirable optoelectronic properties, including strong optical absorption at appropriate (and tunable) wavelengths across the solar spectrum as well as high carrier diffusion length (exceeding 1 μm) and mobility.[3] With absorption coefficients several orders of magnitude greater than silicon, PVSK materials can absorb much more light even at low material thicknesses. These properties are all essential for use in thin-film solar cells, where a small amount of material less than a micron thick must absorb as much light and generate as much charge as possible, and they also make PVSKs potentially useful for other optoelectronic applications, such as light-emitting diodes and lasers.[3]

In general, "perovskite" describes materials with an ABX_3 stoichiometry, with cations A and B and anion X, arranged in a cubic or pseudo-cubic structure with A surrounded by eight vertex-connected BX_6 octahedra (see Fig. 1). Of interest to PV applications are lead halide PVSKs ($B = Pb^{2+}$, $X = Cl^-$, Br^-, I^-) where the A-site cation can be organic, commonly methylammonium ($CH_3NH_3^+$, MA^+) or formamidinium ($HC(NH_2)_2^+$, FA^+), or inorganic, such as Cs^+.

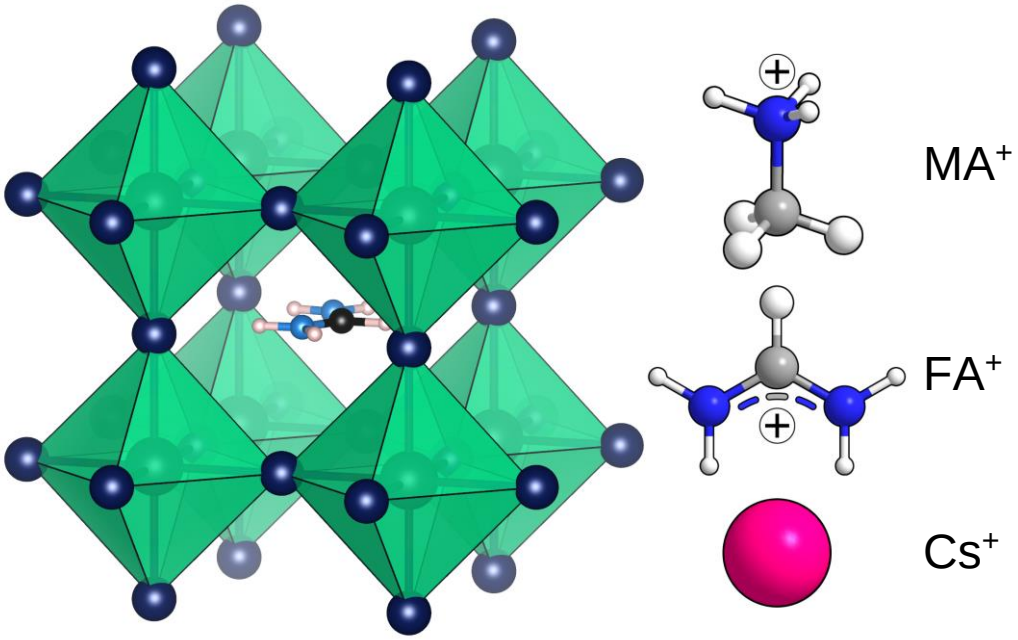

Figure 1. (Left) $FAPbI_3$ PVSK crystal structure (pseudo-cubic, 001 oriented) shown with I^- dark blue Pb^{2+} dark grey, adapted from Weller *et al.*[4], and (right) common choices of A-site cations

Although $MAPbI_3$ is the more well-studied of these configurations, PVSKs employing FA^+ as the A-site cation are of growing interest for their lower band gap (approximately 1.48 eV), more suitable for absorbing in the solar spectrum.[5] This more favorable band gap has allowed the development of highly efficient solar cells with power conversion efficiencies as high as 22.1%.[6] Despite these exciting advancements, PVSK materials still present several challenges. The main issue for these materials as far as applications in solar cells are those of stability, as PVSK films degrade in the presence of moisture, heat, and UV radiation.[7] Intrinsic instability of the PVSK film is another issue that is another real issue affecting the performance of these devices. For instance, FA-PVSKs tend to transition from the useful black α-phase to the yellow δ-phase, but this can be prevented by doping with MABr, giving mixed-halide $FAPbI_{3-x}Br_x$. In this work, an interface-focused approach is taken to improving the conditions (e.g. surface chemical

composition and reactivity, and interfacial crystallinity) for growth of mixed-halide FA-PVSK with more desirable material properties (e.g. increased bulk crystallinity) with a focus on characterization of PVSK physical properties, including a new method employing IR spectroscopy.

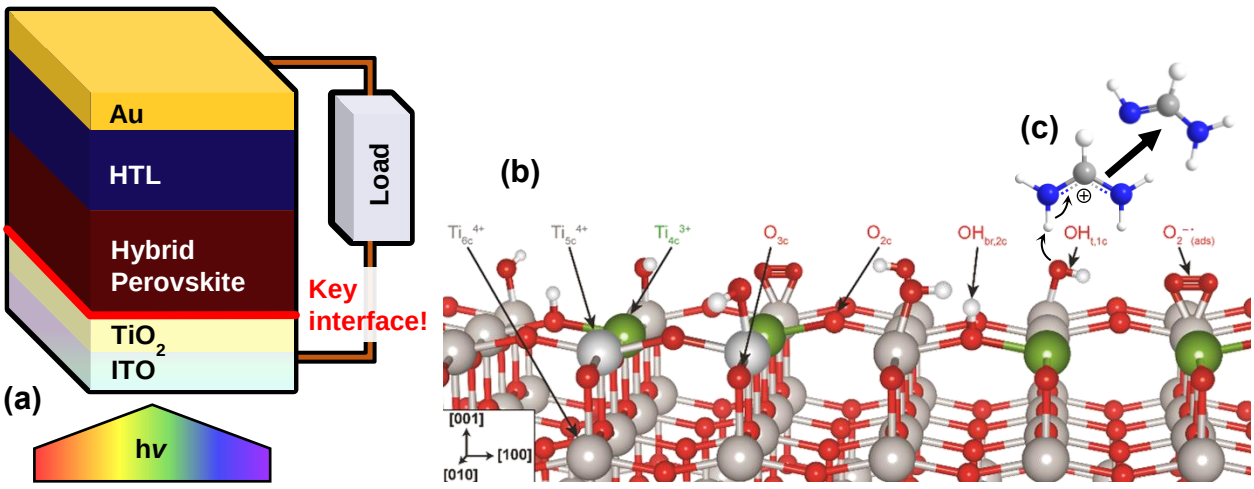

Figure 2. (a) Planar heterojunction PV device architecture, (b) illustration of TiO_2 reactive surface sites, with (c) mechanism for FA^+ degradation by surface hydroxyl

In a typical planar heterojunction solar cell architecture (Fig. 2a), the perovskite is deposited on an electron-selective metal oxide (MO_x) contact, commonly titania (TiO_2). The TiO_2 surface is problematic, however, as it presents a number of defects (surface hydroxyls, under-coordinated Ti_{4c}^{3+} and Ti_{5c}^{4+}, superoxide O_2^-, etc.), as illustrated in Fig. 2b. These defect sites can adversely affect PVSK film growth in several ways since they create a chemically reactive TiO_2 surface. This allows, for instance, deprotonation of the FA^+ cation at the interface by surface or bridging hydroxyls, which could lead to degradation of the PVSK film (Fig 2c). One result of this is lowered PVSK crystallinity due to break down near the interface. In addition, disordered iodide at the interface (at Ti Lewis acid sites), another result of interfacial PVSK degradation, presents a

barrier to charge injection and is linked to current-voltage (*J*-*V*) hysteresis, yet another anomalous property of PVSK materials which negatively impacts device efficiency.[8]

An approach to solving these issues related to instability/reactivity of the TiO2/PVSK interface and, thus, instability of PV devices is the insertion of a thin interlayer of some third compound between the PVSK and the TiO_2 with the goal of (1) passivating chemically reactive TiO_2 surface sites to improve PVSK stability and reduce *J*-*V* hysteresis, (2) presenting a more uniform surface and affording chemical control of that surface for even PVSK crystal growth, and (3) enhancing the hole-blocking capability of the heterojunction to enhance charge extraction. It has been shown, for example, that the incorporation of a thin, conformal layer of [6,6]-phenyl-C_{61}-butyric acid methyl ester (PCBM), commonly used in organic photovoltaics as an electron acceptor, as such allows for high-efficiency, low hysteresis hybrid PVSK PV devices.[9] However, PCBM can only be used as such for vacuum-deposited PVSK films due to its solubility (which increases at higher temperatures) in PVSK processing solvents such as DMF and DMSO.

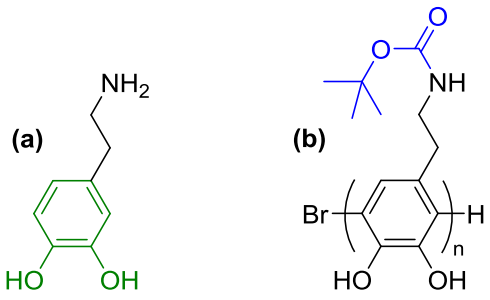

Figure 3. Structures of (a) dopamine, with catechol moiety in green, and (b) BOC-protected polydopamine (n ≈ 23), with BOC group in blue

This work presents a study of dopamine and *tert*-Butyloxycarbonyl (BOC)-protected polydopamine (structures shown in Fig. 3) as surface modifiers for preparation of solution-processed FA-PVSK films on TiO_2 substrates, and characterization of these surface modifiers

and their effects on the properties of the PVSK films. Adsorption of dopamine (Dop) and related compounds to TiO_2 has been studied fairly extensively, in part due to interest in their use as sensitizers in dye-sensitized solar cells and sensors. Of particular interest, it has been shown that the catechol (1,2-benzenediol) moiety can coordinate with TiO_2 in a bridging bidentate (bridging two Ti atoms) mode that allows direct charge injection from the dopamine to the TiO_2 conduction band.[10,11] In addition, dopamine coordination occurs at highly undercoordinated sites at the titania surface, so it is a promising candidate for passivation of these reactive sites.[12] By far the largest challenge in working with Dop, however, is its tendency to oxidize toward more conjugated forms, as shown in Fig. 4.

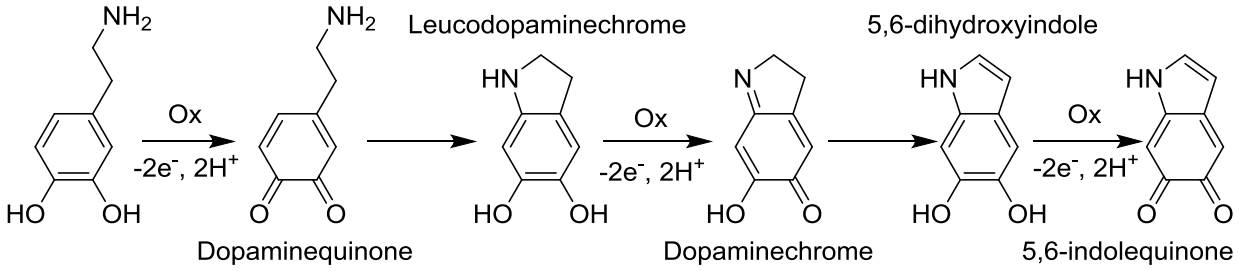

Figure 4. Several steps in the oxidation of dopamine to the indolequinone form[13]

These conjugated forms of dopamine (the dihydroxyindole and indolequinone) can polymerize to form long, conjugated polydopamine or melanin species. Highly oxidized polydopamine, while also useful as a sensitizer,[14] is undesirable for TiO_2 modification in this project for several reasons, including loss of the catechol moiety and increased valence band energy, potentially allowing for hole trapping at the interface. Thus, methods were developed, including pH control and deoxygenation, to prevent this reaction from occurring.

BOC-protected polydopamine[15] (pDop) is also examined as an interlayer material, which is relatively unstudied next to dopamine. pDop is composed of 22-23 monomer units of dopamine

with a BOC protecting group on the amines that prevents ring-closing and oxidation of the polymer to melanin-like polydopamine. This compound is of great interest, as it can more easily form conformal films without losing the catechol functionality as occurs in melanin obtained from autoxidation of dopamine.

In this work, it is shown that dopamine spin-coated on amorphous TiO_2 results in non-conformal coating of the substrate which, after rinsing with DMF, remains as small aggregates concentrated at sites believed to be the most reactive on the surface. On the other hand, pDop forms a conformal, pinhole-free film approximately 5 nm thick that is resistant to solvent rinsing. Both films result in increased crystallinity of FA-PVSK films deposited on these modified substrates when compared those prepared on unmodified TiO_2. In the case of pDop, it also induces an unusual crystal orientation in FA-PVSK growth, the implications of which are yet to be fully characterized.

Important to the advancement of PVSK materials for eventual commercialization is developing techniques to characterize the quality of PVSK films and understand mechanisms of degradation. To that end, this work also details the use of infrared reflection-absorption spectroscopy (IRRAS) to characterize the quality of FA-PVSK films. IRRAS, like the more standard transmission IR spectroscopy, probes vibrational transitions in compounds; however, instead of employing an IR-transparent window, e.g. KBr, the beam is reflected off an underlying substrate, which makes this technique useful for studying thin films.

IR spectroscopy has been used to study PVSK materials, but it is rarely used as a primary technique for characterization and is instead used in a limited scope, and there are many disagreements in the literature (sometimes within a single publication!) about IR spectrum interpretation.[16–18] However, IRRAS is in fact a powerful technique for characterization of these

materials, as it probes only the organic cation (since the PbI_3^- lattice does not exhibit strong vibrational bands in the spectral window). Through careful correlation with X-ray diffraction (XRD), it is shown herein that IRRAS can be used to monitor "free" FA^+ that isn't contained within the PVSK lattice, which is believed to exist at grain boundaries and interfaces between differently oriented crystalline domains in the PVSK film. In this way, IRRAS could be a relatively simple but powerful tool for monitoring PVSK film quality.

II. Methods

Preparation of Dop and pDop films

Commercial indium-doped tin oxide (ITO) on glass substrates (cut to 1" x 1") are cleaned by heated (approximately 70°C) sonication in Triton X-100 (10% v/v in nanopure water), DI water, acetone, and isopropyl alcohol (IPA) for 15 minutes each and then rinsed with IPA and dried under a stream of N_2. Substrates are activated by 20 minute oxygen plasma (OP) treatment (17 W, 700-800 mTorr) using Harrick Scientific PDC-3XG plasma cleaner immediately prior to deposition of amorphous, conformal TiO_2 by chemical vapor deposition (CVD) from titanium(IV) isoproxide in a homebuilt system described previously.[19] 25 minute deposition at 210°C substrate temperature with 0.66 cm^3/min carrier gas flow rate (ultra-high purity N_2) results in nominal film thickness of 30 nm.

Dopamine HCl (m.w. 189.64) is purchased from Sigma-Aldrich and used as received; BOC-protected polydopamine (m.w. 5900 Da) is prepared by collaborators through previously reported process.[15] All solvents are degassed by bubbling with argon prior to use, and depositions should be performed under low-light to prevent oxidation of Dop and pDop species. A 5 mg/mL solution of Dop or pDop is prepared by dissolving 5 mg sample in 1 mL degassed, nanopure water adjusted to appropriate pH (6.5 for Dop / 3.5 for pDop) by addition of dilute HCl. Prior to use, these solutions are filtered through a 0.45 μm PVDF syringe filter. CVD-TiO_2 substrates are cut to ½" x ½" and activated by oxygen plasma for 10 minutes, and then Dop or pDop films are immediately deposited by spin-coating (35 μL aliquot, 4000 rpm, 4000 rpm/s, 60 s). Films are then transferred to a N_2 glovebox and heated at 100°C for 20 min on a hotplate to anneal films and drive off surface-bound water.

Rinsed films are prepared as follows, in a N_2 glovebox. A 93 μL/mL dilution of dimethyl sulfoxide (DMSO) in dimethyl formamide (DMF) is filtered through a 0.25 μm PTFE syringe filter and heated to 105°C in a vial on a hotplate. Annealed ITO/CVD-TiO_2/(Dop or pDop) films are rinsed with three 30μL aliquots of solvent while spinning at 6000 rpm for 60 s. Rinsed films are heated at 70°C on a hotplate for 10 min while purging the glovebox with fresh N_2 to drive off excess solvent.

Preparation of FA-PVSK films

MAX-doped (X=Br^-, or Cl^-, I^-) FA-PVSK films are prepared in the glovebox from solution on Dop/pDop-modified or unmodified CVD-TiO_2 substrates by a procedure that has been described in detail previously.[20] The method is a two-step interdiffusion-adduct approach where a PbI_2-DMSO adduct film is deposited from a 1.3 M (each) solution in DMF, followed by an FAI:MAX film deposited from IPA.[21,22] Films are annealed in DMSO atmosphere (solvent vapor anneal, SVA) by heating at 150°C for 60 min in a covered glass petri dish containing 20 μL DMSO, affording high-quality FA-PVSK films. Films may also be annealed in N_2 atmosphere (thermal anneal, TA) without adding DMSO solvent.

Film Morphology with AFM and SEM

Atomic force microscopy (AFM) is used to gather a topographical profile of film surfaces with nanometer resolution. AFM is gathered on a Digital Instruments Multimode SPM with Nanoscope III controller in PeakForce Tapping mode with Scanasyst tips. In AFM, a microscopic needle is moved across the sample surface while piezoelectric controllers cause it to tap the surface. A laser is reflected off the needle tip, and deflection of the laser measures the

force experienced by the needle, which reports on the height of the film. AFM is a powerful technique for obtaining a nanometer-resolution heightmap of a film.

Scanning electron microscopy (SEM) is an imaging technique where a beam of electrons is focused on the sample surface, and the scattered electrons are detected. By raster scanning the beam across a section of the surface, images of very high magnification can be obtained. This technique is much faster than AFM and thus more useful for studying some aspects of film morphology, but does not give quantitative height information. SEM is used to study PVSK films to search for pinholes and examine grain size. Images are gathered on a Hitachi S-4800 High Resolution SEM.

Film Characterization by IR Spectroscopy

IRRAS and transmission IR spectra are gathered on a Thermo Nicolet Magna-IR 550 Series II FTIR spectrometer with liquid N_2-cooled mercury cadmium telluride (MCT) detector and Parker Balston Model 75-45 purge gas generator. IRRAS measurements are made with a Spectra-Tech FT-80 Fixed 80° Grazing Angle accessory with a circular 7 mm diameter sample mask, and a linear polarizer is used to achieve *p*-polarization (E-field parallel to plane of incidence) of the IR beam. When spectra are gathered, the substrate is placed film-side-down on the sample mask and weighted with a 70 g weight to be sure it lays flat, and the chamber is allowed to purge for five minutes before spectra are gathered (1 cm^{-1} resolution, 300 scans, approx. 7 min). It is always necessary to gather a background spectrum of the correct underlying substrate (i.e. Glass/ITO/CVD-TiO_2) to ensure the background and sample have the same substrate reflectance. Spectra are background-corrected in Fityk.[23]

Surface Characterization by PES

Photoelectron spectroscopy (PES) is a technique for analysis of surface composition and energetics. Electrons are ejected from a sample by irradiation with either an X-ray source (XPS) or a UV source (UPS). By analyzing the abundances and binding energies of core- and valence-shell electrons, an idea of the chemical makeup and surface interactions and energetics is obtained. Surface modification of TiO_2 is analyzed by PES on a Kratos 165 Ultra Photoelectron Spectrometer with Al kα X-ray source and a HeI and HeII UV source.

PVSK Film Characterization by X-ray Diffraction

X-ray diffraction (XRD) is used to characterize the crystallinity and crystal orientation of PVSK films. In a regularly ordered atomic lattice, X-rays are diffracted at specific angles related to the lattice plane spacing. This provides a method for measuring overall order in a PVSK film, which is generally a desirable property for efficient charge generation. Powder diffraction (2θ-scan) XRD spectra of PVSK films on modified and unmodified TiO_2 on a Philips X'pert MPD. Prior to XRD analysis, films are encapsulated in poly(methy methacrylate) (PMMA) by spin-coating 15 mg/mL PMMA solution in chlorobenzene (25μL, 4000 rpm, 4000 rpm/s, 20 s) in an N_2 glovebox.

III. Results & Discussion

Dop and pDop Film Characterization

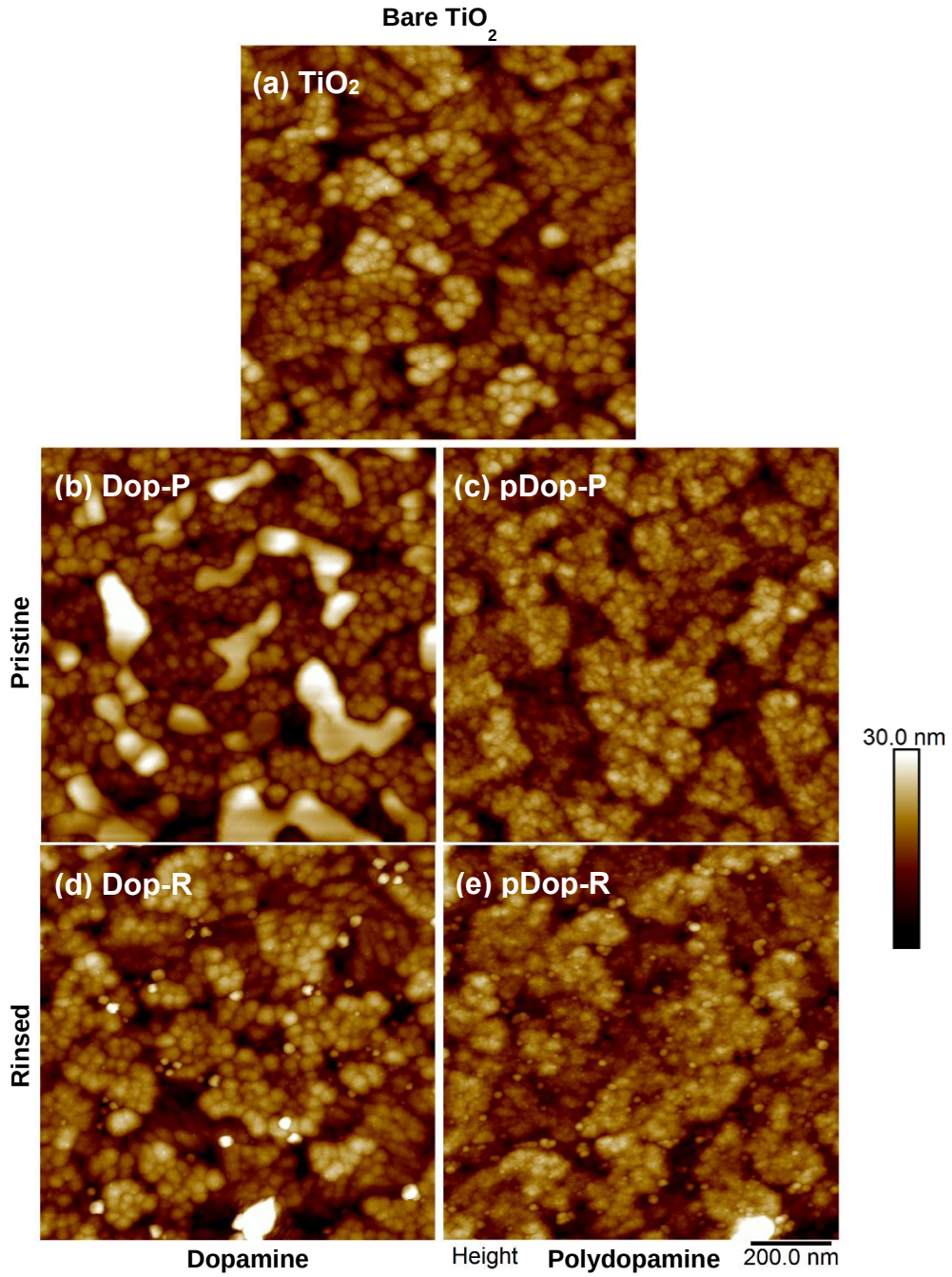

Figure 5. AFM topographical images of Dop and pDop films in comparison with (a) bare TiO_2, showing both (b-c) pristine [-P] and (d-e) rinsed [-R] films, after rinsing with DMSO/DMF

AFM images of Dop and pDop films on TiO_2 (Fig. 5) reveal an interesting picture of the compounds' interactions at the TiO_2 surface. In the pristine films, Dop (Fig 5a) is seen to not coat the TiO_2 substrate conformally; instead, the film exhibits island-like growth, with 10-20 nm tall deposits of Dop mainly occurring in depressions in the TiO_2 surface. After rinsing, as shown in Fig. 5d, Dop is mostly washed away, and the sample resembles unmodified TiO_2 with small (20-30 nm diameter) features distributed across the surface. These features, believed to be dopamine or dopamine aggregates, are concentrated mainly at the step-edges of the TiO_2, where reactive surface defects occur most. This suggests dopamine selectively binds at the reactive sites on the TiO_2 surface which we wish to target, which is very promising.

On the other hand, Fig. 5c shows pDop coats the TiO_2 evenly (preserving the substrate morphology) and seemingly without pinholes. This is likely due to several differences between monomeric and polymeric dopamine. For instance, as a small molecule, dopamine can aggregate more easily, allowing island formation. The BOC group on pDop also contains a fairly Lewis-basic carbonyl group that may bind to TiO_2 more favorably than the catechol. Upon rinsing, pDop (unlike Dop) remains coating the substrate, but similarly to the rinsed Dop films, features resembling aggregates are seen on the surface, mainly concentrated at the edges of TiO_2 features and in depressions on the film surface (Fig 5e). This is a good indication for pDop's use as a surface modifier, as a true interlayer must not wash away during PVSK deposition.

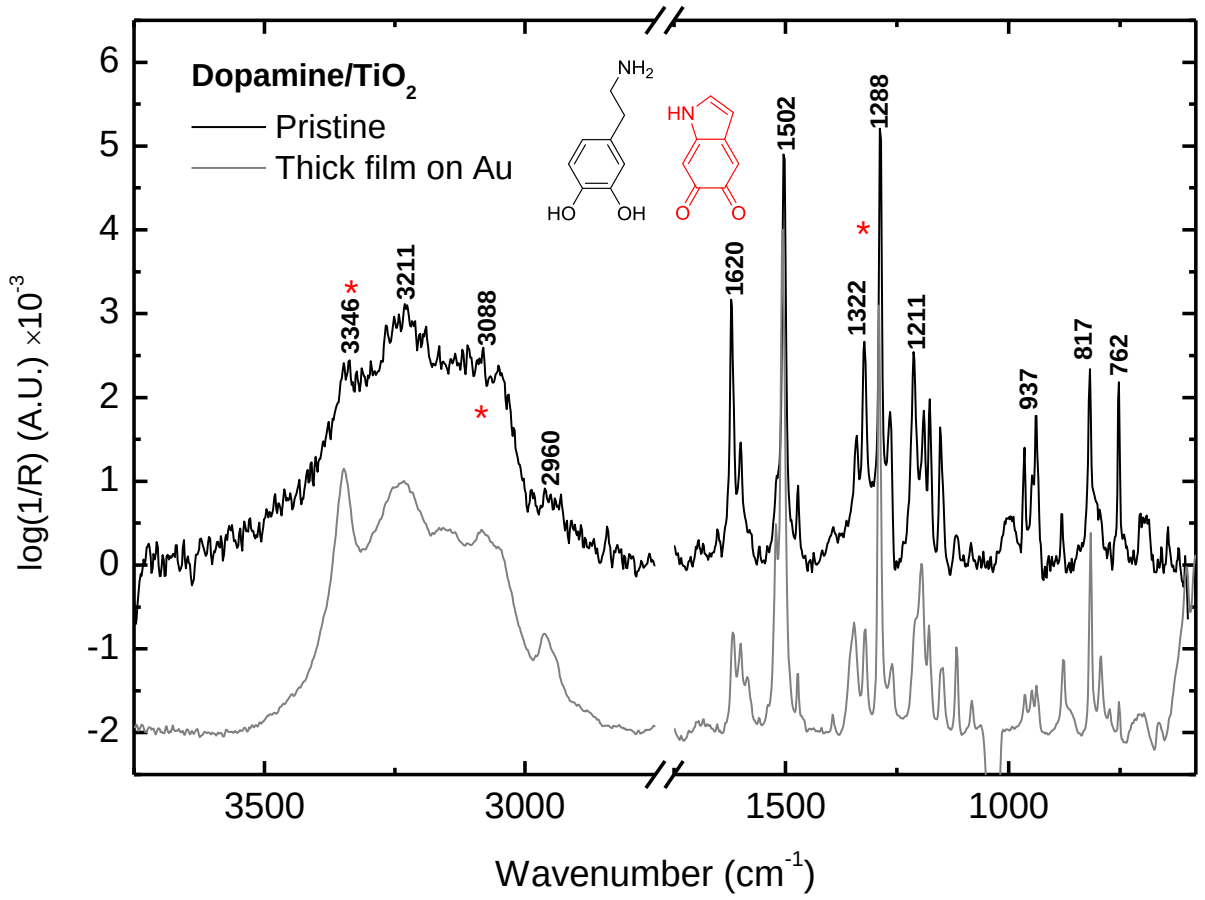

Figure 6. IRRAS spectrum of Dop film on TiO_2 with peaks labeled and dopamine and oxidized dopamine structure shown; IRRAS spectrum of thick (10 mg/mL) Dop film on Au shown for reference; peak assignment right

ν (cm^{-1})	**Assignment**[24,25]
3346	$\nu(NH_2)_{asym}$
3211	$\nu(NH_2)_{sym}$, ν(NH), ν(OH)
3088	$\nu(CH_{arom})$
2960	$\nu(CH_2)$
1620	ν(C=O), $\nu(C{=}C_{arom})$
1502	$\nu(C{=}C_{arom})$
1322	ρ(COH)
1288	ν(C-O)
1211	ρ(COH)
937	ν(C-C-N)
817	$\delta(CH_{arom})$
762	Ring

ν, ρ, and δ, designate stretch, in-plane bend, out out-of-plane bend, respectively.

The IRRAS spectrum of Dop-TiO_2 reveals information about dopamine's structure in the film. Of note, there does appear to be partial oxidation of the dopamine in the film, evidenced by the prominence of the ν(C=O) band at 1620 cm^{-1}, and a reduction in the intensity of both the asymmetric ν(NH_2) at 3346 cm^{-1}, as the primary amine is converted to a secondary amine, and the aromatic ν(CH_2) at 2960 cm^{-1}, as aliphatic carbon in the ethylamine moiety becomes aromatic. For comparison, Fig. 6 shows the IRRAS spectrum of a pristine film on a gold substrate prepared from a 10 mg/mL solution of dopamine, which shows the primary differences in peaks as outlined above.

This oxidation not unexpected, as dopamine is known to oxidize and polymerize at the TiO_2 surface, which has been exploited for use in photocatalysts and dye-sensitized solar cells.[13,14] As such, it is unclear whether this oxidation would present a problem for the use of a Dop interlayer in PVSK solar cells. Indeed, it may be that this species, which cannot bind covalently to the TiO_2 surface due to the loss of the catechol moiety, is largely washed away upon rinsing the film, but currently that is unknown; further characterization of these surfaces must focus on this fact.

Note, additionally, that polydopamine formed *in situ* as such differs from the pDop examined in this study in several ways. Most importantly, BOC-protection of the amine in the pDop sample prevents oxidation, not only through ring-closing of the ethylamine moiety, but also by preventing loss of the catechol to the quinone form, which, without the proceeding ring-closing step, is reversible. In addition, the pDop used in this study has a very low polydispersity index (Đ=1.02) at a molecular weight of 5900 Da, corresponding to a length of approximately 23 monomer units.[15] On the other hand, this precision cannot be guaranteed by generation of polydopamine at the TiO_2 surface, and thus this reaction at least represents an undesirable loss of

control. In many ways, pDop in this study is an attempt to take advantage of the desirable properties of polydopamine without sacrificing control by proceeding through *in situ* generation.

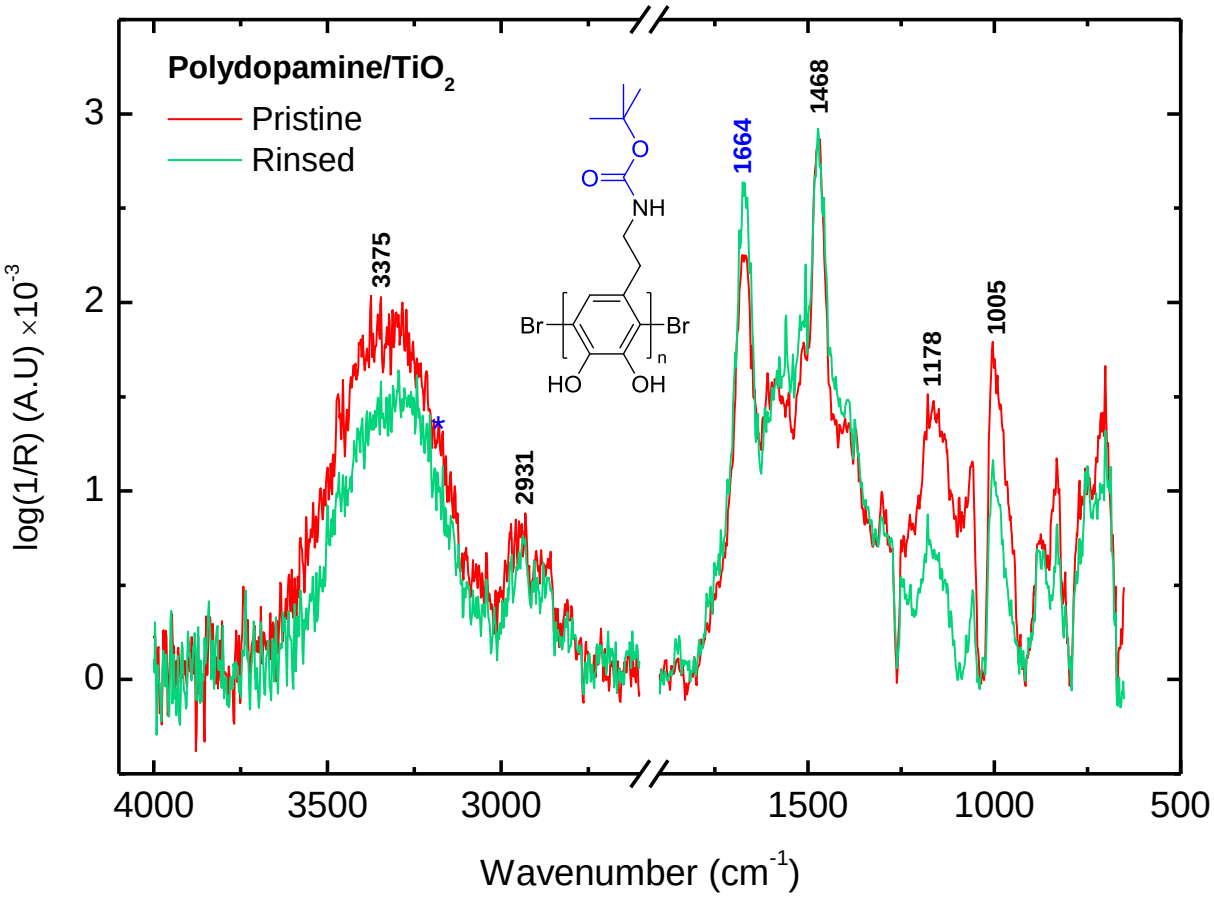

Figure 7. IRRAS spectrum of pDop film on TiO_2 pristine and rinsed with DMSO/DMF, with peaks labeled and pDop structure shown; peak assignment right

υ (cm^{-1})	**Assignment**
3375	ν(NH), ν(OH), ν(CH_{arom})
2931	ν(CH_2), ν(CH_3)
1664	ν(C=O)
1468	ν(C=C_{arom})
1178	
1005	

ν designates stretch

The IRRAS spectra of pDop-TiO_2 indicates that the amine remains primarily BOC-protected, as evidenced by the strong presence of the ν(C=O) band at 1664 cm^{-1}, as well as the relatively high intensity of the aliphatic ν(CH) band at 2931, due to both the *tert*-butyl termination of the BOC-group and the lack of ring-closing as seen in dopamine that would result in formation of aromatic CH stretching. In comparison with literature spectra of bulk polydopamine, the peaks retain their shape (less broadening) which suggests that extended polymerization has not occurred.

In addition, the IRRAS further indicates that rinsing the pDop films does not remove much of the film. It is difficult to quantify with this technique, however, due to the low signal-to-noise and uneven baseline. For more thorough characterization of this surface, PES is employed.

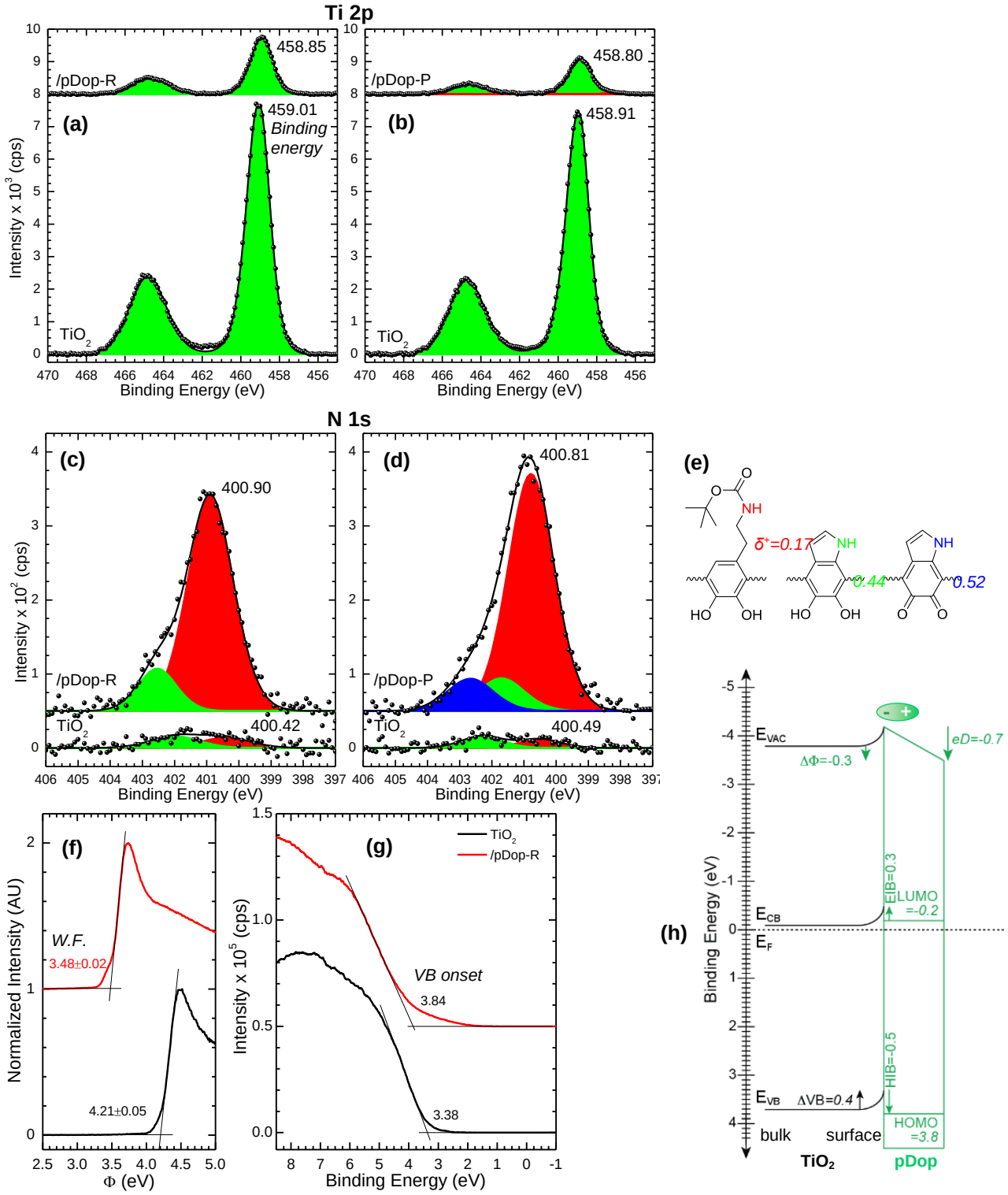

Figure 8. Stacked PES spectra comparing pDop pristine [-P] and rinsed [-R] films on TiO_2; (a-b) Ti 2p and (c-d) N 1s XPS spectra with (e) peak assignments by extended Huckel charge approximation; UPS spectra of rinsed films, showing (f) work function and (g) valence band onset windows; (h) band energy diagram of pDop-TiO_2 interface

Seen in Fig. 8, XPS and UPS data inform on the composition and energetics of the pDop film and the underlying TiO_2 surface. In Fig. 8a and 8b, deposition of the pDop film (both pristine and rinsed) is seen to attenuate the Ti 2p signal, and shift the Ti 2p 3/2 peak by -0.11 and -0.16 eV on the pristine and rinsed films, respectively. Because titanium is exclusively found in the TiO_2 substrate, attenuation of this signal is exponentially related to the thickness of the film, described by the following equation:[26]

$$d = \ln\frac{I_0}{I}\lambda_n cos\theta$$

where I_0 and I are the Ti 2p signal (fitted area) from the bare TiO_2 and the TiO_2/pDop films, respectively, λ_n is the inelastic mean free path of the photoelectron (2.79 nm for a Ti 2p photoelectron generated by an Al kα source traveling through an organic overlayer), and θ is the take-off angle relative to the surface normal (0°). For the TiO_2/pDop films, this gives a thickness of 5.4 nm pristine and 4.3 nm after rinsing, showing approximately 1 nm is rinsed off the film. This is thicker than a monolayer but is thin enough that it wouldn't be expected to interfere with electron extraction, which speaks well for application of this material in solar cells.

The slight shift in the Ti 2p 3/2 peak upon addition of the pDop film (approx. -0.1 eV) indicates slight de-doping, or oxidation, of the TiO_2 surface by the polymer film. This is unexpected, as TiO_2 tends to reduce upon addition of an organic overlayer; the implications of this shift are unclear and require further characterization – and possibly mitigation – if pDop is to be used in solar cell devices.

The N 1s XPS spectra (Fig. 8c & 8d) support the observation from the IRRAS spectra that much of the pDop film is still BOC-protected (the primary fitted peak), although there is a sizeable

contribution from what are believed to be oxidized (melanin-like) species at higher binding energies, assigned by extended Huckel approximations of the charge on the amine, as higher charge leads to higher binding energy. A change in the peak shape after rinsing is explained by a loss of one of the species (the middle peak, poly-5,6-dihydroxyindole) which may suggest, as suggested earlier, that binding occurs through the BOC group as opposed to the catechol.

The UPS data in Fig. 8f show a large (approximately -0.7 eV) shift in the work function (the energy required to remove an electron from the surface to vacuum) indicating that the pDop surface presents a positive surface dipole, which makes for a more electron-rich surface amenable to PVSK nucleation and growth. The valence band (VB) onset in Fig. 8g increases by 0.46 eV from bare TiO_2 to pDop-TiO_2. From the UPS data in Fig. 8f and 8g and the Ti 2p binding energy in Fig. 8b, taking the optical absorbance onset of pDop to be approximately 4.0 eV (from preliminary UV/Vis spectra, not shown), a rough energy level diagram is constructed for the TiO_2-pDop interface, shown in Fig. 8h, according to an analytical schema outlined in a to-be-published manuscript from colleagues in this group.[26] Fig. 8h shows that the TiO_2/pDop contact has enhanced hole blocking capability (-0.5 eV hole injection barrier, HIB) compared to the bare TiO_2, which aids in the charge selectivity of the contact, and therefore potentially could improve device performance. There is a slight (0.3 eV) electron injection barrier (EIB), which isn't desired at this contact, but before a more precise band diagram can be constructed, it is not enough to discount pDop as an interlayer material. pDop thus appears to provide a favorable energetic environment at the TiO_2 contact; however, telling data is found in the actual characterization of PVSK films deposited on these substrates.

Dop and pDop Effects on PVSK Films

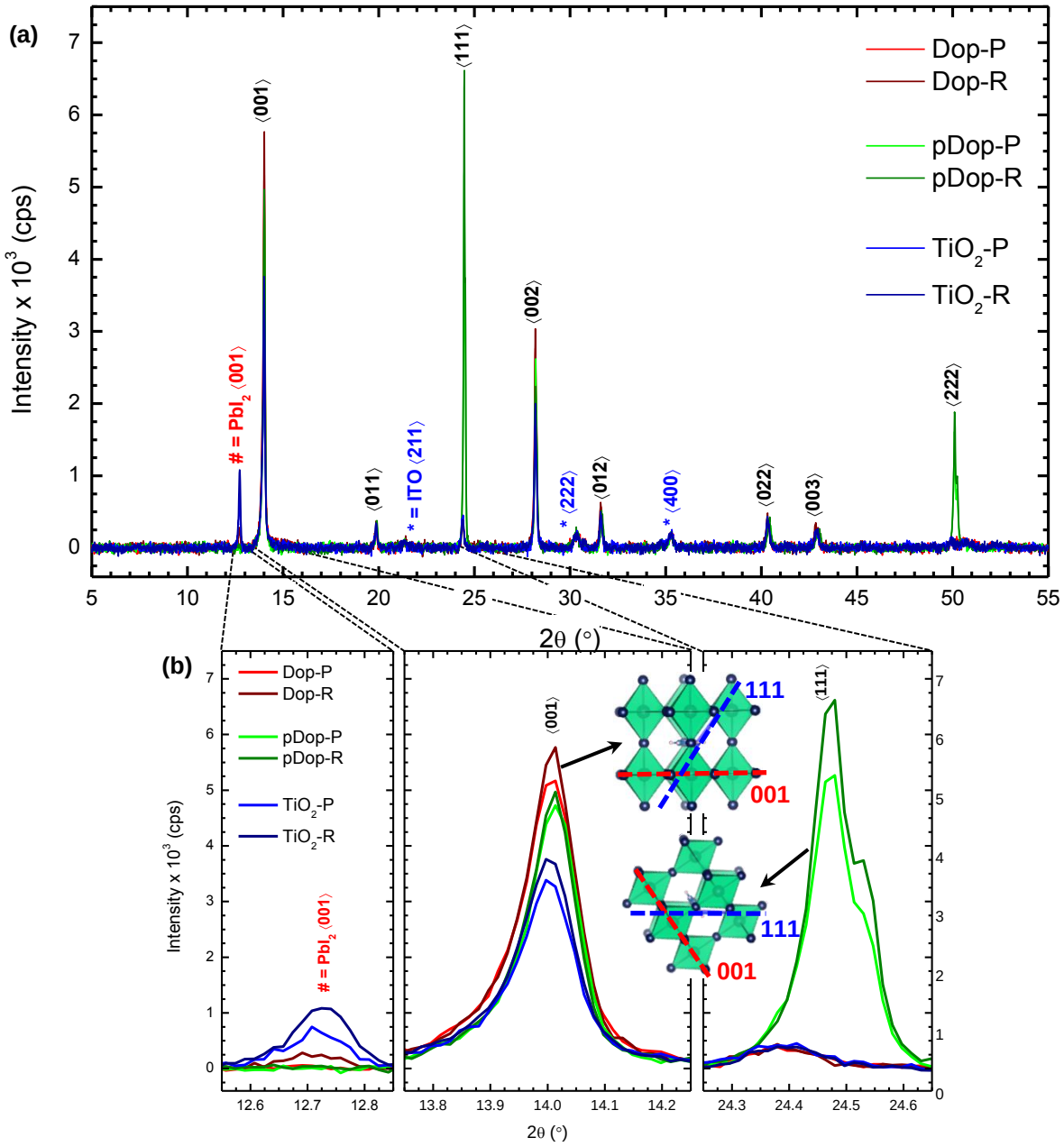

Figure 9. Representative XRD spectra, (a) full and (b) zoomed on three peaks of interest, of FA-PVSK films prepared on bare TiO_2, TiO_2/Dop, and TiO_2/pDop, pristine and rinsed; average peak intensities from repeated measurements in table right

	XRD Peak Intensity		
Sample	**PbI_2 (001)**	**FA-PVSK (001)**	**FA-PVSK (111)**
Dop-P	75 ± 21	5560 ± 280	388 ± 19
Dop-R	258 ± 25	5490 ± 300	439 ± 65
pDop-P	75 ± 12	4940 ± 200	5110 ± 700
pDop-R	63 ± 21	4500 ± 380	9400 ± 4200
TiO_2-P	697 ± 39	3230 ± 190	466 ± 22
TiO_2-R	1070 ± 120	3790 ± 130	429 ± 36

The XRD data (Fig. 9) show a notable increase in PVSK crystallinity (i.e. greater peak intensity/area) in films deposited on Dop- and pDop-modified TiO_2 over those on unmodified substrates. Generally, FA-PVSK with a cubic structure is (001) oriented, so an increase in the associated peak intensity indicates a more crystalline film. On both Dop- and pDop-modified TiO_2, such an increase is seen, with as high as a 75% increase on pristine Dop to a 20% increase on rinsed pDop, over bare TiO_2 (Table 3). This change is especially surprising for the rinsed Dop film, where the amount of dopamine remaining on the film is very small, and yet the PVSK (001) peak shows a 44% increase in intensity. This further supports the claim that Dop on this TiO_2 surface is selectively binding to the most reactive sites on the TiO_2 substrate, preventing decomposition of the PVSK at the interface which in turn templates more uniform crystal growth and higher-quality PVSK films.

Fig. 9b shows a few peaks of interest. PVSK films on the modified substrates exhibited lower intensity in the PbI_2 (001) peak, indicative of unconverted precursor, with all but rinsed Dop (where the peak still showed a marked decrease from unmodified TiO_2) exhibiting negligible peak intensity for this structure. This suggests chemical passivation of the TiO_2 surface by these modifiers, preventing the deprotonation of FA^+ at the interface which results (stoichiometrically) in excess PbI_2. Excess PbI_2 may in fact be beneficial to solar cell performance, but this effect is poorly understood and may be due to interface effects (which Dop- and pDop-modification aim to solve separately) or secondary advantageous effects.[27]

By far the most surprising result from this XRD data is the enormous intensity of the PVSK (111) peak in PVSK samples on pDop-TiO_2. Typically this peak is small, as in the Dop and bare TiO_2 samples, and regarded as an “impurity”, indicative of domains that are oriented differently than the bulk of the film. On pDop-TiO_2, both pristine and rinsed, however, this is the primary

XRD peak with greater intensity than even the PVSK (001) peak. The pDop interlayer must in some fashion template growth of the PVSK in this unusual orientation. While this structure has been reported on in a limited scope before, whether or not it brings about desirable physical properties is unclear, so this finding represents an interesting future direction for the study of pDop as an interlayer.[28]

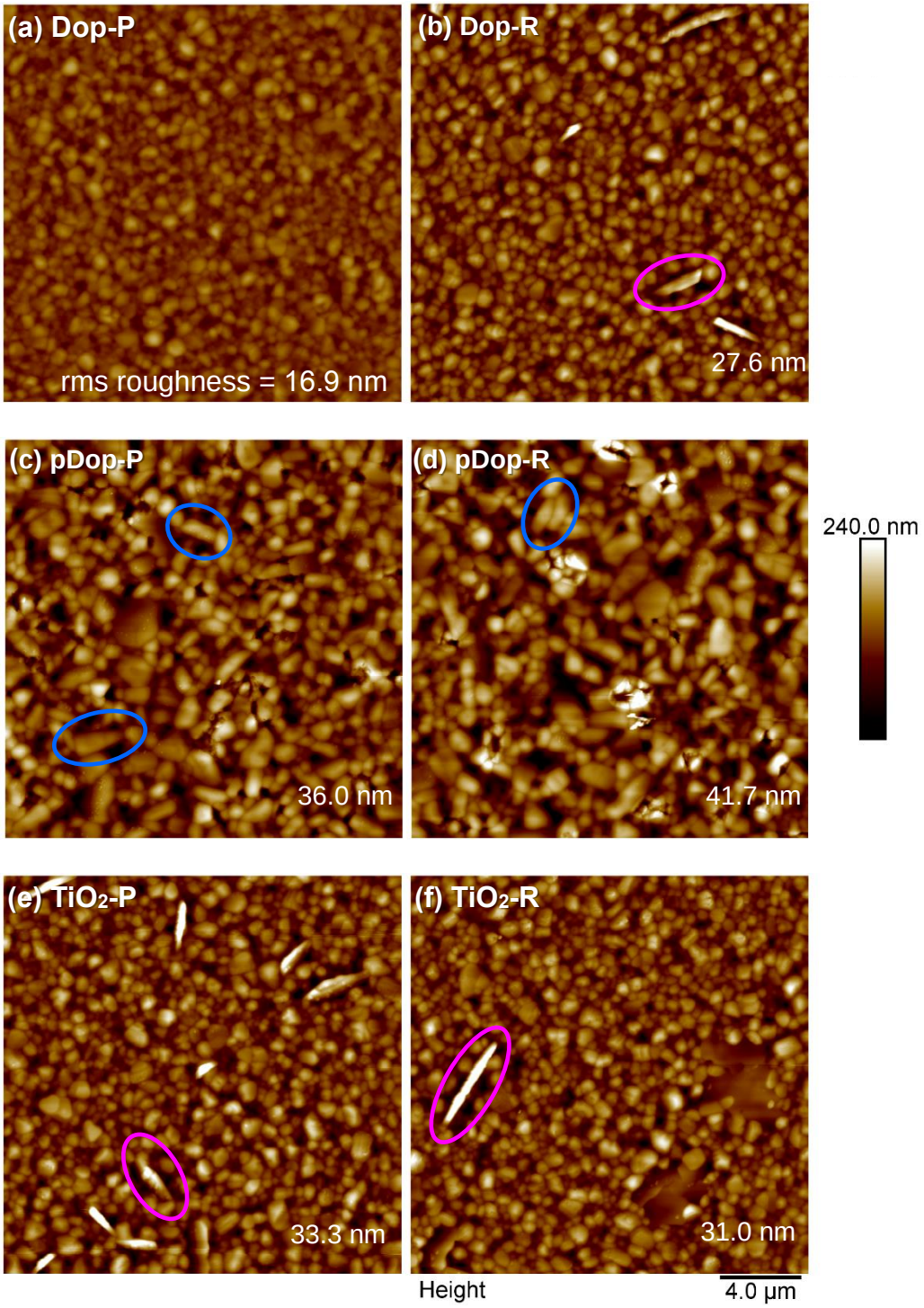

Figure 10. AFM topographical images of FA-PVSK films (after encapsulation with PMMA) on pristine [-P] and rinsed [-R] substrates of (a-b) TiO_2/Dop, (c-d) TiO_2/pDop, and (e-f) bare TiO_2, with rms roughness displayed. Circled in magenta are PbI_2 domains (b,e,f) and in blue are high aspect-ratio PVSK grains (c,d)

AFM topographical images (Fig. 10) of the PVSK films were collected to study morphological changes induced by modification, and these images show some remarkable corroboration of the XRD data. On the pristine Dop-TiO_2 substrates, the PVSK films showed the smallest grain sizes (note the low rms roughness), while the rinsed Dop-TiO_2 substrate resulted in similar morphology to the bare TiO_2, including the emergence of large PbI_2 domains, which were observed in XRD spectra, circled in magenta in Fig. 10b, 10e, & 10f. It seems that the large amount of Dop at the surface when the precursors are spun onto the pristine substrate results in smaller grain size due to Dop acting as a contaminant (similarly to adventitious carbon on an unclean substrate). Rinsing away this excess results in a "cleaner" surface that more resembles the bare TiO_2, so grain growth proceeds normally from a morphological standpoint, but, as shown in the XRD data, with significantly enhanced crystallinity.

The pDop-TiO_2 substrates caused the most dramatic morphological changes in the PVSK film, with much larger grain sizes and greatest rms roughness. Without a full grain analysis, it is difficult to comment on the dispersity of grain size in these films relative to bare TiO_2 PVSKs; however, the presence of high aspect ratio ("long") grains, circled in blue in Fig. 10c and 10d, in these films is noted visually, in comparison to the predominantly low aspect ratio ("round") grains in the other two sample sets. This morphological distinction could be evidence of the (111) oriented PVSK domains that dominate the XRD spectra of these films; a different mode of crystal growth results in different grain morphology.

FTIR Characterization of FA-PVSK

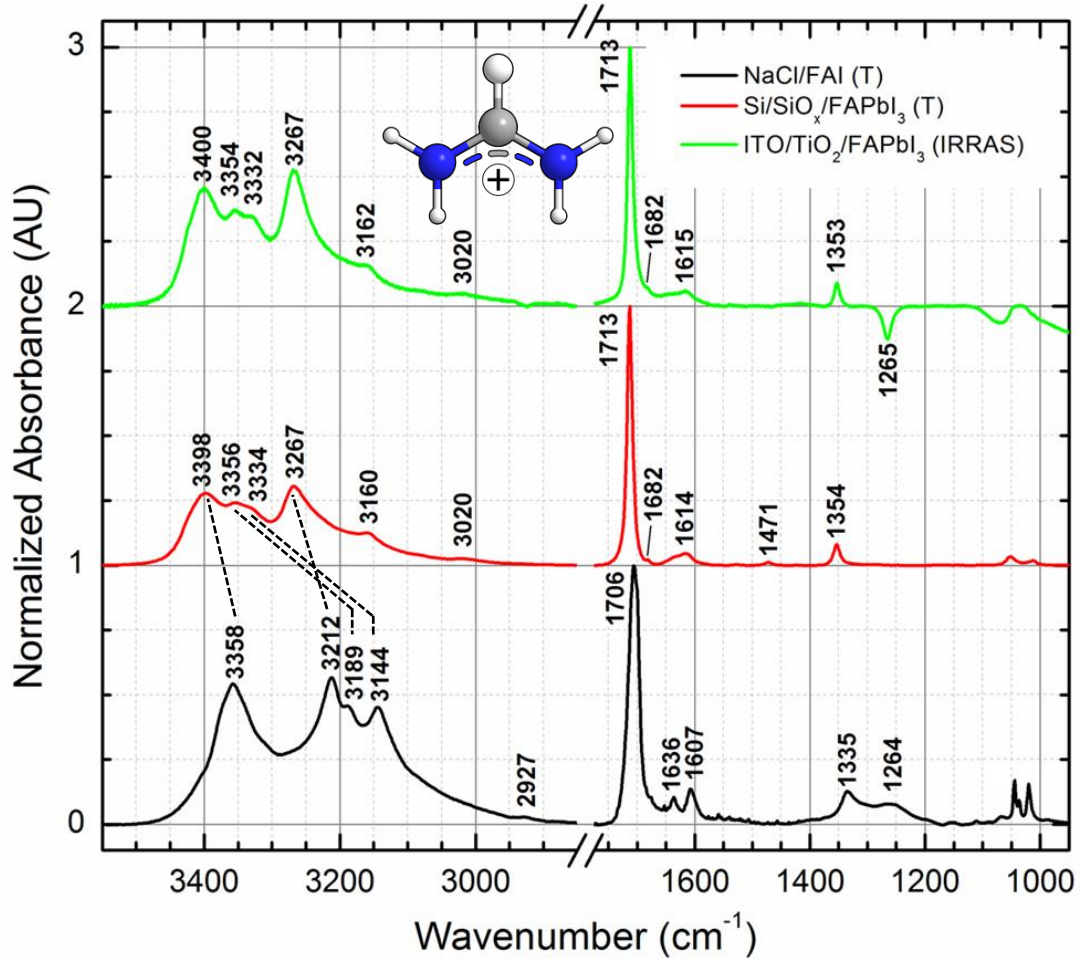

Figure 11. Comparison of normalized IRRAS and transmission IR (T) spectra of FA-PVSK films with T-IR spectrum of FAI precursor salt; cation structure above and peak assignment in table right

ν (cm^{-1}) FAI (T)	ν (cm^{-1}) FA-PVSK (T)	ν (cm^{-1}) FA-PVSK (IRRAS)	Assignment
1264		1265	ν(C-O)
1335	1354	1353	ν(C-N)
	1471		
1607	1614	1615	ρ(NH_2)
1636	1682	1682	ρ(CH)
1706	1713	1713	ν(C=N)
2927	3020	3020	
	3160	3162	
3212	3267	3267	ν(CH)
3144	3334	3332	ν(NH_2)$_{sym}$
3189	3356	3354	ν(NH_2)$_{asym}$
3358	3398	3400	ν_1

ν and ρ designate stretching and in-plane bending, respectively

IRRAS has proven a surprisingly useful tool for characterization of FA-PVSK films, especially as a method of monitoring the FA^+ cation. Fig. 11 presents a comparison between the transmission IR spectrum of FAI (the precursor salt) and the transmission IR spectrum (obtained by preparing the film on an IR-transparent silicon wafer) and IRRAS spectrum of FA-PVSK which has surprising implications that thus far have been overlooked in the literature. Note in both the FAI and FA-PVSK spectra, the primary peak at 1706-1713 cm^{-1} is attributed to ν(C=N) – though a more proper designation may be $\nu(C\text{-}N)_{asym}$, with a transition dipole moment parallel to the N↔N axis, which is more fitting of the equivalence (through resonance) of the two amine groups.[17] There is a slight shift toward higher energy in the peak position from the precursor salt to the PVSK film; this effect is by far more dramatic, however, in the group stretching region, 3500-3000 cm^{-1}, where shifts of 40-180 cm^{-1} can be seen.

This shift is most pronounced for the $\nu(NH_2)$ modes, which can be explained by hydrogen bonding. The effect of hydrogen bonding on vibrational spectra is complex, but generally hydrogen bonding shifts X-H stretching to lower frequencies, and increases the intensity of these bands.[29] This suggests, then, that hydrogen bonding is stronger in the FAI precursor than in the PVSK film. Indeed, it has previously been shown that hydrogen bonding between the amines of FA^+ and lattice I^- occurs in the PVSK structure[4,30]; however, in crystalline FAI, the amines and iodide can achieve better coaxial alignment and closer proximity, resulting in a stronger hydrogen bond.[31]

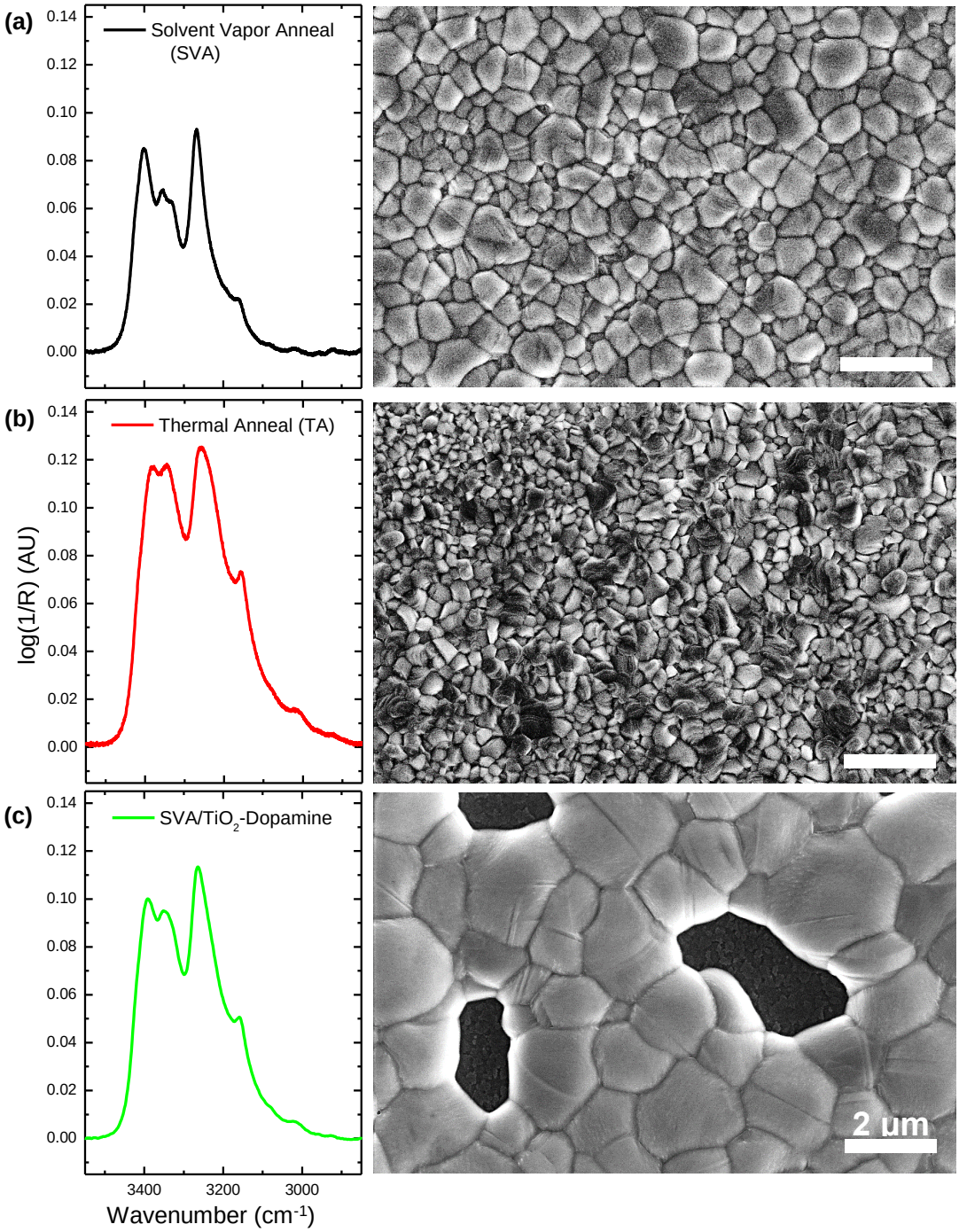

Figure 12. IRRAS spectra group stretching region (left) and SEM images (right) of FA-PVSK films; (a) solvent vapor annealed and (b) thermally annealed films on TiO_2, and (c) an early attempt at FA-PVSK deposition on TiO_2-Dop that showed de-wetting and formation of pinholes

With this effect in mind, it is not surprising that this region of the IR spectrum can vary significantly between films, as shown in Fig. 12 above. By changing the processing conditions (e.g. annealing the film with and without the presence of solvent vapor) or altering the TiO_2 surface, as shown with an early PVSK on Dop-TiO_2 film, large morphological changes can be induced that in turn cause changes in the IR spectrum, as shown. In general, there is a trend toward minimization of the IR band intensity in this region, especially of the $\nu(NH_2)$ modes, in "good" PVSK films, i.e. those with large grains and complete coverage. In Fig. 12b, thermal annealing led to small grain sizes (and thereby many grain boundaries), while in Fig. 12c, poor surface wetting allowed large PVSK grains to form, but resulted in very large (>2 μm diameter) pinholes across the film. In both cases, the IRRAS spectrum shows increased absorbance in this region, particularly in the $\nu(NH_2)$ bands, and through the lens of hydrogen bonding the reason becomes clear. In lower-quality films, IRRAS is reporting on the presence of "free" FA^+, which more closely resembles the precursor FAI, and as the data suggests this seems to reside at grain boundaries (or the edges of pinholes) where the PVSK crystal structure terminates.

This effect has been noted in the literature in a limited extent in organotin perovskites, where the IR spectrum of a fresh FA-SnI_3 film showed increased absorption (similar to Fig _ c) compared to the same film after 12 h in air.[32] The explanation given for this was that hydrogen bonding with water caused decrease absorption, which may seem contrary to the assertions herein; however, when considering the strength of an N-H$\cdots OH_2$ hydrogen bond versus N-H$\cdots I^-$, it seems that the introduction of water to the would decrease hydrogen bonding, leading to the observed decrease in IR absorption. Thus, this proposed explanation is consistent with previously reported results.

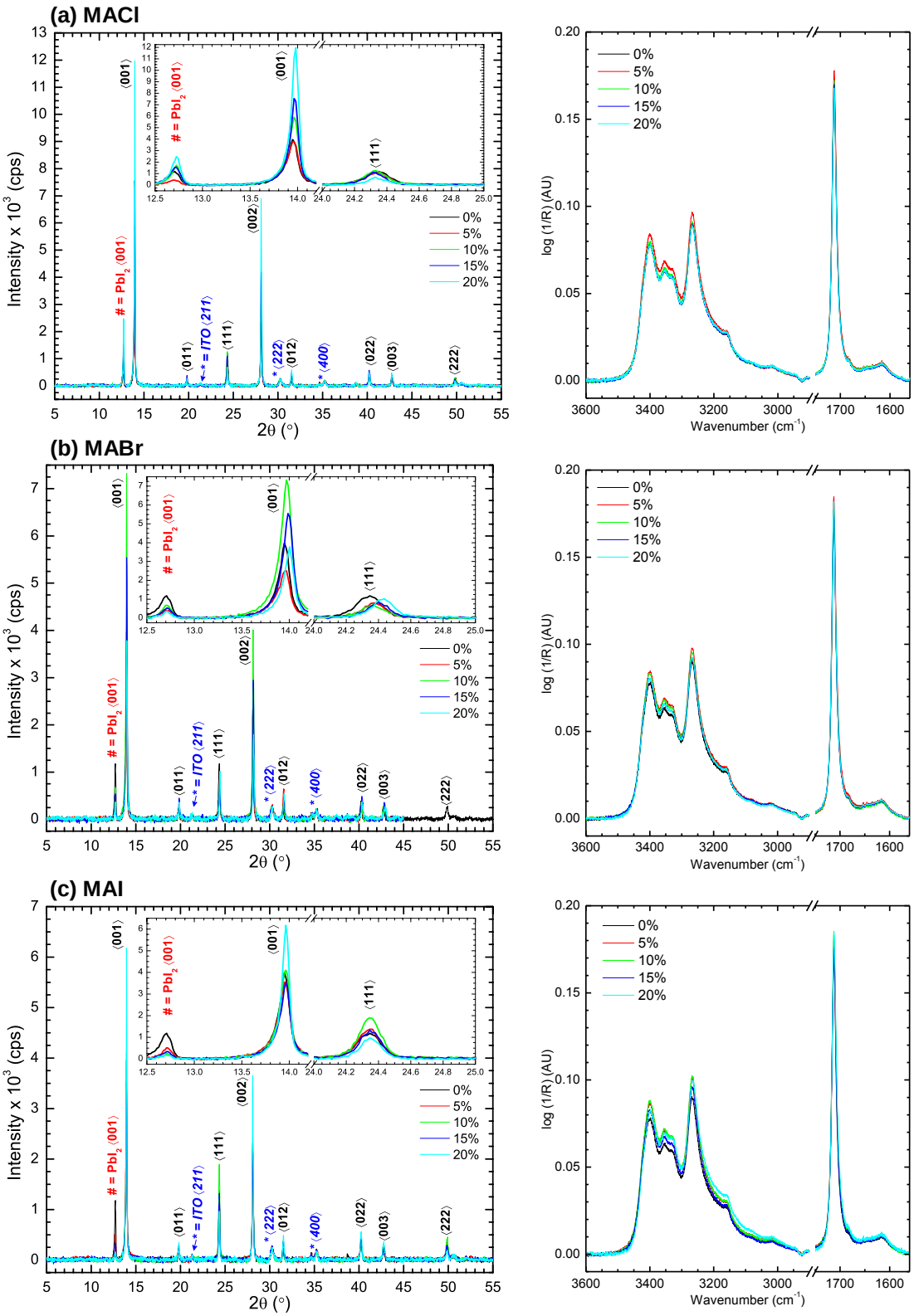

Figure 13. XRD spectra with peaks of interest inset, and IRRAS spectra with group stretching region and ν(C=N) shown for (a) MACl, (b) MABr, and (c) MAI-doped FA-PVSK films on TiO_2

To quantify the observed effect, FA-PVSK films doped with various amounts of MACl, MABr, and MAI, (0-20 mol%) were prepared in order to induce structural changes in the PVSK, and the films were characterized by XRD and IRRAS, shown in Fig. 13. The peaks of interest in the XRD spectra are the (001) peak, which is the primary orientation, and the (111) peak, which in this case represents domains that adopt an irregular orientation. In MACl- and MAI-doped PVSK films, the (001) orientation is seen to increase with increasing dopant, while in MABr-doped PVSK films the intensity peaks at 10% and then falls again. More important in this data is the (111/001) peak ratio, which reports on the average crystallite orientation (i.e. a higher ratio indicates less overall order due to relatively high presence of (111) oriented regions).

In the IRRAS spectra, there are shifts in the 3500-3000 cm^{-1} region corresponding to changes in dopant concentration, though they are subtle. To elucidate trends in this data, the peak intensities are plotted against the (111/001) ratio described above.

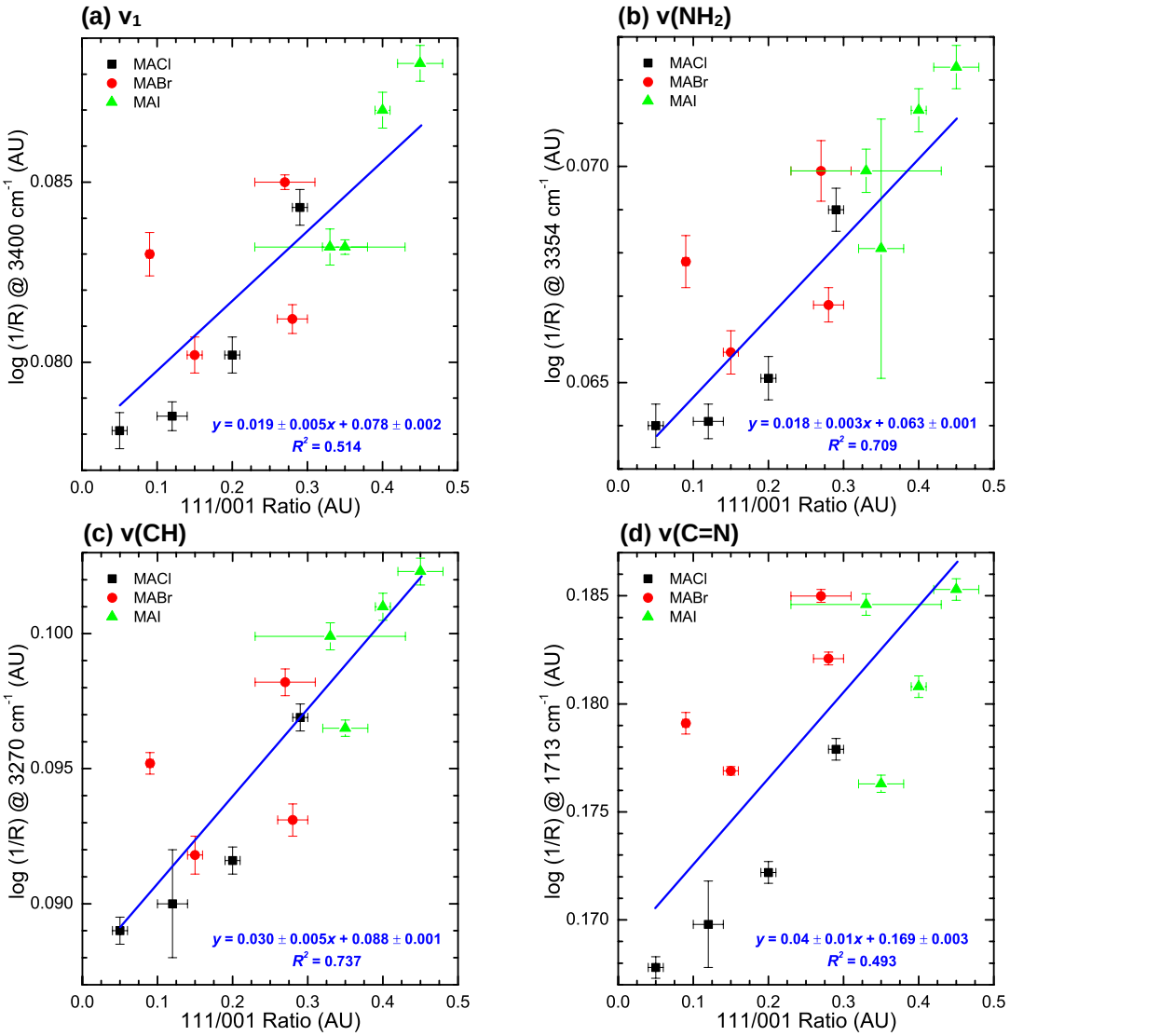

Figure 14. IRRAS intensity vs (111/001) ratio from XRD spectra for MAX-doped FA-PVSK films, shown for (a-d) four IR transitions, as labeled; (e) illustration of proposed explanation for this trend

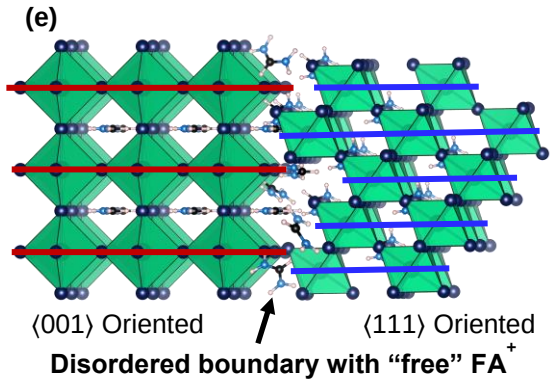

It is seen in Fig. 14 that there is a reasonably strong relationship between the (111/001) ratio and the intensity of the IR absorptions of the FA-PVSK film. This trend is pronounced for the $\nu(NH_2)$ and ν(CH) modes, which supports the assertion that this effect is due to hydrogen bonding of the FA^+ cation with I^-, which affects X-H stretching modes most. It seems in films with a higher (111/001) ratio, there are more domains in the (111) orientation, and as such there is a greater amount of twinned regions (illustrated in Fig. 14e), where the two differently-oriented domains interface. The data suggests the presence of "free" FA^+ (so-called because it is not contained in the PVSK lattice structure, associated with halogen anions for charge balance) at these boundaries, which has not before been reported. This could have large implications on PVSK PV device functionality, where ion migration within disordered regions (e.g., at the TiO2/PVSK interface, PVSK grain boundaries and twinned PVSK interfaces where different crystal orientations meet) is considered a contributor to *J-V* hysteresis[8] and instability of PV devices.

IV. Conclusions & Future Directions

Both dopamine and BOC-protected polydopamine show promise as interlayer materials for passivation of TiO_2 in planar heterojunction perovskite solar cells. While Dop does not coat the TiO_2 surface conformally, the small amount left on the surface after rinsing seems to bind preferentially to what should be the most reactive sites, and indeed large increases, as high as 75% greater (001) intensity, are observed in FA-PVSK crystallinity on Dop-modified TiO_2 contacts. This is particularly exciting, as dopamine has the potential to passivate reactive TiO_2 sites while not interfering with charge extraction, which could bode well for its application in PV devices. There are many variables that could still be studied, such as solution pH (i.e. protonating and deprotonating the dopamine amine), to study its effects on PVSK film growth.

pDop modification presents a more complicated picture, with many potential directions of study. pDop allows for conformal, pinhole-free coating of the TiO_2 surface, with film thickness around 5.4 nm, and after rinsing, the bulk of the film (approximately 4.3 nm) remains. While the binding mode of this compound to TiO_2 is unclear, what is important is that through surface passivation, it seems to prevent chemical degradation of the PVSK by reactive TiO_2 surface sites. In addition, the TiO_2 surface energetics are broadly affected by pDop modification; a large, positive surface dipole and increased hole-blocking capability both indicate potential for increasing PV device performance. In addition, pDop modification results in increased PVSK crystallinity and effects a remarkable change in the preferred orientation of the PVSK film to boot. Characterization of the PVSK film near this surface would help explain this phenomenon and could be a very interesting future study. pDop as an interlayer presents unknowns that still need to be resolved by more extensive characterization, and perhaps development of new film processing procedures, but it is certainly an interesting material that could be highly useful in PVSK PV applications.

Lastly, through careful IRRAS characterization of FA-PVSK films, an interesting new picture of the cation's properties in the film has been uncovered. IR spectroscopy is arguably underused in the literature as a technique for analyzing these materials, while it is shown in this work that it can be very powerful in detecting the presence of free FA^+, an indicator of film quality. As a relatively low-cost technique, one could imagine its use, for example, in an industrial setting as a tool to monitor PV device quality during manufacturing. Further work in this area will concentrate on better understanding of formamidinium vibrational modes (e.g. through theoretical calculation) for a complete assignment of the IR spectrum.

Acknowledgements

In addition my advisor, Dr. Neal Armstrong, who helped immensely to guide this project and help me develop skills as a researcher, this work would not have been possible without the help of Dr. R. Clayton Shallcross. Both through helping to design run experiments and teaching me how to better interpret and present data, Dr. Shallcross has aided not only in this project but in improving my ability to perform, and perhaps more importantly understand, science. I also thank graduate students Kara Saunders and Jimmy Stanfill for making my time in the Armstrong group an enjoyable and memorable experience.

References

(1) Kojima, A.; Teshima, K.; Shirai, Y.; Miyasaka, T. Organometal Halide Perovskites as Visible-Light Sensitizers for Photovoltaic Cells.

(2) National Renewable Energy Labs (NREL) efficiency chart https://www.nrel.gov/pv/assets/images/efficiency-chart.png (accessed Apr 19, 2018).

(3) Chen, Q.; De Marco, N.; Yang, Y. (Michael); Song, T.-B.; Chen, C.-C.; Zhao, H.; Hong, Z.; Zhou, H.; Yang, Y. Under the Spotlight: The Organic–inorganic Hybrid Halide Perovskite for Optoelectronic Applications. *Nano Today* **2015**, *10* (3), 355–396.

(4) Weller, M. T.; Weber, O. J.; Frost, J. M.; Walsh, A. Cubic Perovskite Structure of Black Formamidinium Lead Iodide, A‑[HC(NH 2) 2]PbI 3 , at 298 K.

(5) Eperon, G. E.; Stranks, S. D.; Menelaou, C.; Johnston, M. B.; Herz, L. M.; Snaith, H. J. Formamidinium Lead Trihalide: A Broadly Tunable Perovskite for Efficient Planar Heterojunction Solar Cells.

(6) Yang, W. S.; Park, B.-W.; Jung, E. H.; Jeon, N. J.; Kim, Y. C.; Lee, D. U.; Shin, S. S.; Seo, J.; Kim, E. K.; Noh, J. H.; et al. Iodide Management in Formamidinium-Lead-Halide-Based Perovskite Layers for Efficient Solar Cells. *Science* **2017**, *356* (6345), 1376–1379.

(7) Wang, D.; Wright, M.; Elumalai, N. K.; Uddin, A. Stability of Perovskite Solar Cells. *Sol. Energy Mater. Sol. Cells* **2016**, *147*, 255–275.

(8) Azpiroz, J. M.; Mosconi, E.; Cd, J. B.; De Angelis, F. Defect Migration in Methylammonium Lead Iodide and Its Role in Perovskite Solar Cell Operation. *Energy Environ. Sci. Energy Environ. Sci* **2118**, *8* (8), 2118–2127.

(9) Tao, C.; Neutzner, S.; Colella, L.; Marras, S.; Ram, A.; Kandada, S.; Gandini, M.; De Bastiani, M.; Pace, G.; Manna, L.; et al. 17.6% Stabilized Efficiency in Low-Temperature Processed Planar Perovskite Solar Cells. *Energy Environ. Sci. Energy Environ. Sci* **2015**, *8* (8), 2365–2370.

(10) Syres, K.; Thomas, A.; Bondino, F.; Malvestuto, M.; Grätzel, M. Dopamine Adsorption on Anatase TiO $_2$ (101): A Photoemission and NEXAFS Spectroscopy Study. *Langmuir* **2010**, *26* (18), 14548–14555.

(11) Tae, E. L.; Lee, S. H.; Lee, J. K.; Yoo, S. S.; Kang, E. J.; Yoon, K. B. A Strategy To Increase the Efficiency of the Dye-Sensitized TiO 2 Solar Cells Operated by Photoexcitation of Dye-to-TiO 2 Charge-Transfer Bands.

(12) Redfern, P. C.; Zapol, P.; Curtiss, L. A.; Rajh, T.; Thurnauer, M. C. Computational Studies of Catechol and Water Interactions with Titanium Oxide Nanoparticles.

(13) Zangmeister, R. A.; Morris, T. A.; Tarlov, M. J. Characterization of Polydopamine Thin Films Deposited at Short Times by Autoxidation of Dopamine.

(14) Nam, H. J.; Kim, B.; Ko, M. J.; Jin, M.; Kim, J. M.; Jung, D.-Y. A New Mussel-Inspired Polydopamine Sensitizer for Dye-Sensitized Solar Cells: Controlled Synthesis and Charge Transfer. *Chem. - A Eur. J.* **2012**, *18* (44), 14000–14007.

(15) Repenko, T.; Fokong, S.; De Laporte, L.; Go, D.; Kiessling, F.; Lammers, T.; Kuehne, A. J. C. Water-Soluble Dopamine-Based Polymers for Photoacoustic Imaging. *Chem. Commun.* **2015**, *51* (28), 6084–6087.

(16) Dimesso, L.; Quintilla, A.; Kim, Y.-M.; Lemmer, U.; Jaegermann, W. Investigation of

Formamidinium and Guanidinium Lead Tri-Iodide Powders as Precursors for Solar Cells. *Mater. Sci. Eng. B* **2016**, *204*, 27–33.

(17) Taylor, V. C. A.; Tiwari, D.; Duchi, M.; Donaldson, P. M.; Clark, I. P.; Fermin, D. J.; Oliver, T. A. A. Investigating the Role of the Organic Cation in Formamidinium Lead Iodide Perovskite Using Ultrafast Spectroscopy.

(18) Park, B.; Philippe, B.; Jain, S. M.; Zhang, X.; Edvinsson, T.; Rensmo, H.; Zietz, B.; Boschloo, G. Chemical Engineering of Methylammonium Lead Iodide/Bromide Perovskites: Tuning of Opto-Electronic Properties and Photovoltaic Performance. *J. Mater. Chem. A* **2015**, *3* (43), 21760–21771.

(19) Ou, K.-L.; Tadytin, D.; Xerxes Steirer, K.; Placencia, D.; Nguyen, M.; Lee, P.; Armstrong, N. R. Titanium Dioxide Electron-Selective Interlayers Created by Chemical Vapor Deposition for Inverted Configuration Organic Solar Cells. *J. Mater. Chem. A* **2013**, *1* (23), 6794.

(20) Shallcross, R. C.; Zheng, Y.; Saavedra, S. S.; Armstrong, N. R. Determining Band-Edge Energies and Morphology-Dependent Stability of Formamidinium Lead Perovskite Films Using Spectroelectrochemistry and Photoelectron Spectroscopy. *J. Am. Chem. Soc.* **2017**, *139* (13), 4866–4878.

(21) Xiao, Z.; Bi, C.; Shao, Y.; Dong, Q.; Wang, Q.; Yuan, Y.; Wang, C.; Gao, Y.; Huang, J. Efficient, High Yield Perovskite Photovoltaic Devices Grown by Interdiffusion of Solution-Processed Precursor Stacking Layers. *Energy Environ. Sci.* **2014**, *7* (8), 2619–2623.

(22) Jo, Y.; Oh, K. S.; Kim, M.; Kim, K.-H.; Lee, H.; Lee, C.-W.; Kim, D. S. High

Performance of Planar Perovskite Solar Cells Produced from PbI_2 (DMSO) and PbI_2 (NMP) Complexes by Intramolecular Exchange. *Adv. Mater. Interfaces* **2016**, *3* (10), 1500768.

(23) Wojdyr, M. Fityk: A General-Purpose Peak Fitting Program. *J. Appl. Cryst.* **2010**, *43*, 1126–1128.

(24) Gunasekaran, S.; Kumar, R. T.; Ponnusamy, S. Vibrational Spectra and Normal Coordinate Analysis of Adrenaline and Dopamine. *Indian J. Pure Appl. Phys.* **2007**, *45*, 884–892.

(25) Lagutschenkov, A.; Langer, J.; Berden, G.; Oomens, J.; Dopfer, O. Infrared Spectra of Protonated Neurotransmitters: Dopamine. *Phys. Chem. Chem. Phys.* **2011**, *13* (7), 2815–2823.

(26) Shallcross, R. C.; Olthof, S.; Meerholz, K.; Armstrong, N. R. Chemical Interactions and Reactions between Vacuum-Deposited Methylammonium Lead Iodide (MAPbI3) Perovskite Active Layers and TiO2 Contacts. **2018**.

(27) Jesper Jacobsson, T.; Correa-Baena, J.-P.; Halvani Anaraki, E.; Philippe, B.; Stranks, S. D.; F Bouduban, M. E.; Tress, W.; Schenk, K.; Moser, J.-E.; Rensmo, kan; et al. Unreacted PbI 2 as a Double-Edged Sword for Enhancing the Performance of Perovskite Solar Cells.

(28) Cheng, Z.; Lin, J. Layered Organic–inorganic Hybrid Perovskites: Structure, Optical Properties, Film Preparation, Patterning and Templating Engineering.

(29) Bratož, S.; Hadži, D. Infrared Spectra of Molecules with Hydrogen Bonds. *J. Chem. Phys.*

J. Chem. Phys. J. Chem. Phys. J. Chem. Phys. J. Chem. Phys. J. Chem. Phys. **1957**, *27* (131).

(30) Kanno, S.; Imamura, Y.; Hada, M. Theoretical Study on Rotational Controllability of Organic Cations in Organic−Inorganic Hybrid Perovskites: Hydrogen Bonds and Halogen Substitution. *J. Phys. Chem. B* **2017**, *121*, 26188–26195.

(31) Petrov, A. A.; Goodilin, E. A.; Tarasov, A. B.; Lazarenko, V. A.; Dorovatovskii, P. V.; Khrustalev, V. N.; IUCr. Formamidinium Iodide: Crystal Structure and Phase Transitions. *Acta Crystallogr. Sect. E Crystallogr. Commun.* **2017**, *73* (4), 569–572.

(32) Wang, F.; Ma, J.; Xie, F.; Li, L.; Chen, J.; Fan, J.; Zhao, N. Organic Cation-Dependent Degradation Mechanism of Organotin Halide Perovskites. *Adv. Funct. Mater.* **2016**, *26* (20), 3417–3423.